Diagn Interv Radiol 2022; DOI: 10.5152/dir.2022.211100

CHEST IMAGING

ORIGINAL ARTICLE

Indeterminate pulmonary subsolid nodules in patients with no history of cancer: growing prediction, CT pattern, and pathological diagnosis

Xiaowan Guo
Xudong Jia
Danqing Zhang
Hui Feng
Yana Dou
Gaofeng Shi

PURPOSE
We aimed to evaluate and compare the growth patterns among pathological types of indeterminate subsolid nodules in patients without a history of cancer as observed on computed tomography (CT).

METHODS
This retrospective study included 77 consecutive patients with 80 indeterminate subsolid nodules on unenhanced thin-section CT. Subsolid nodules were classified into 2 growth pattern groups based on volume: growth (n = 35) and non-growth (n = 42). According to the pathological diagnosis, subsolid nodules were further subdivided into 3 groups: adenocarcinoma in situ (growth, n = 8 vs. non-growth, n = 22), minimally invasive adenocarcinoma (n = 14 vs. n = 15), and invasive adenocarcinoma (n = 13 vs. n = 5). Kaplan–Meier and Cox proportional hazards regression analyses were performed to identify the risk factors for subsolid nodules growth. The CT findings of the 35 subsolid nodules in the growth group were compared among the 3 pathological groups.

RESULTS
In the growth group, the overall mean volume doubling time and mass doubling time (MDT) were 811.5 days and 616.5 days, respectively. Patient's age (odds ratio = 1.041, $P = .045$) and CT subtype of non-solid nodule and part-solid nodule (odds ratio = 3.430, $P = .002$) could predict subsolid nodule growth. The baseline volume, mass, and mean CT value were larger in the invasive adenocarcinoma group than in the adenocarcinoma in situ group (all $P < .01$). The shortest volume doubling time was observed in the invasive adenocarcinoma group, followed by the minimally invasive adenocarcinoma group and the adenocarcinoma in situ group. A shorter mass doubling time was observed in the minimally invasive adenocarcinoma group than in the adenocarcinoma in situ group (all $P < .02$).

CONCLUSION
As age increases, the risk of pulmonary subsolid nodule growth increases by 4% each year, and part-solid nodules have a 3 times higher risk of growth compared to non-solid nodules in patients with no history of cancer. Subsolid nodules with more aggressive pathological characteristics grow at a faster rate.

From the Department of Computed Tomography and Magnetic Resonance (X.G., H.F., G.S. ✉ gaofengshi2020@163.com), Hebei Medical University Fourth Affiliated Hospital and Hebei Provincial Tumor Hospital, Shijiazhuang, Hebei Province, China; Department of Radiology (X.G., D.Z.), Hebei General Hospital, Shijiazhuang, Hebei Province, China; Department of Urology (X.J.), Hebei Medical University No2 Hospital: Second Hospital of Hebei Medical University, Shijiazhuang, Hebei Province, China; Siemens Healthineers (Y.D.), Beijing, Shanghai, China.

Received 3 November 2021; revision requested November 29, 2021; last revision received January 19, 2022; accepted 26 February 2022.

DOI: 10.5152/dir.2022.211100

Incidentally detected pulmonary subsolid nodules (SSNs) can commonly present as indeterminate nodules on chest computed tomography (CT) in routine workflows. Pulmonary SSNs can be divided into non-solid nodules (NSNs) and part-solid nodules (PSNs) according to the absence or presence of internal solid components on thin-section CT, respectively.[1,2] Subsolid nodules can be benign or malignant; most benign SSNs can be radiologically diagnosed based on whether the lesion resolves on follow-up CT scans, while a few persistent SSNs must be surgically confirmed as focal organizing pneumonia and non-specific interstitial fibrosis.[3] Pulmonary SSNs that persist after a follow-up period of 3-6 months have a high likelihood of being premalignant or malignant lesions, and many authors consider persistent SSNs to represent early-stage adenocarcinoma or its precursor.[3-5] However, it is still important to determine the following: (1) the growth patterns of radiologically malignant SSNs, (2) what growth patterns can be identified on imaging, and (3) whether the imaging pattern corresponds to the pathological type.

You may cite this article as: Guo X, Jia X, Zhang D, Feng H, Dou Y, Shi G. Indeterminate pulmonary subsolid nodules in patients with no history of cancer: growing prediction, CT pattern, and pathological diagnosis. *Diagn Interv Radiol.* 2022;28(3):230-238.

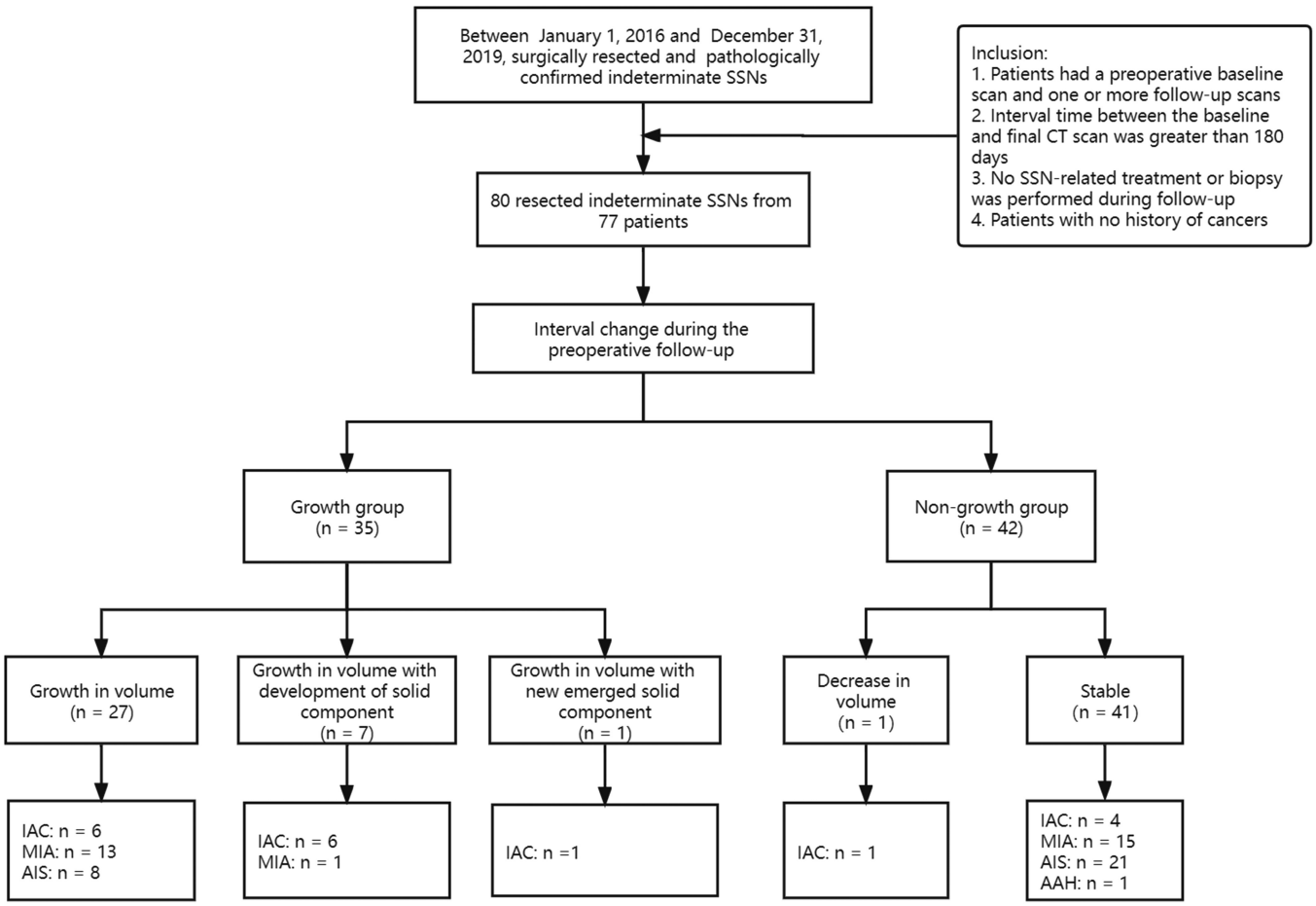

Figure 1. Flowchart of the study population. SSN, subsolid nodule; IAC, invasive adenocarcinoma; MIA, minimally invasive adenocarcinoma; AIS, adenocarcinoma in situ; AAH, atypical adenomatous hyperplasia.

Main points

- Imaging growth patterns of pathological types of pulmonary subsolid nodules (SSNs) as indeterminate lesions observed on chest computed tomography (CT) in routine workflows were evaluated and compared among patients without a history of cancer.
- Pulmonary SSNs on CT scans could be classified into growth or non-growth imaging patterns; the growth pattern tends to have invasive pathology, while the non-growth pattern is indicative of non-invasive findings.
- The risk of pulmonary SSN growth increases with age; SSNs with more aggressive pathological characteristics grow at a faster rate, and part-solid nodules are more likely to grow compared with non-solid nodules.
- The imaging growth patterns observed on the pre-surgical chest CT scans in this study can potentially assist radiologists, oncologists, and surgeons in managing indeterminate SSNs in clinical practice.

Previous studies on the growth patterns of pulmonary SSNs have some limitations. Some did not observe any growth because of the short follow-up period,[6-8] and other studies included patients both with and without a history of cancer, even though cancer history appears to be a risk factor for pulmonary SSN growth.[9-11] A few studies did not share these limitations, but postoperative pathological data were obtained for only a limited number of patients, so the influence of pathological type on pulmonary SSNs could not be comprehensively determined.[12,13]

The present study evaluated the risk of the growth of indeterminate SSNs in patients without a history of cancer and compared the growth pattern on CT with the pathological type.

Methods

Our study implemented measures and a risk management plan for the use of medical technology to guarantee patient safety in clinical research projects formulated by the institution. This study was approved by the ethics committee of our hospital (NO. 202049), and the institutional review committee waived the requirement for informed consent.

Study population

Consecutive patients with pathologically confirmed SSNs who underwent chest CT examinations at our hospital or the physical examination center from January 1, 2016, to December 31, 2019, were included. Patients who met the following criteria were enrolled: (1) preoperative baseline scan and 1 or more follow-up scans; (2) time interval between the baseline and final CT scan longer than 180 days; (3) no SSN-related treatment or biopsy performed during follow-up; and (4) no previous malignancy. Figure 1 presents the patient inclusion flow chart. One radiologist (5 years of experience in chest radiology) searched and recorded the clinical data, radiological findings, and pathological diagnoses of all patients.

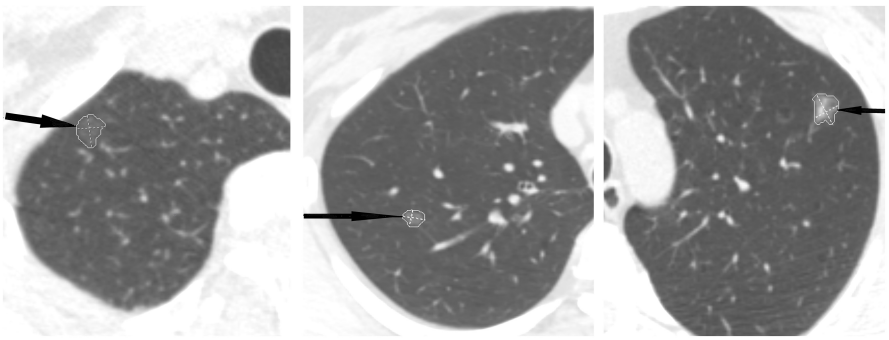

Figure 2. Different SSN shapes were segmented manually by delineating the ground-glass margin slice by slice on all axial images.

Computed tomography imaging and subsolid nodules subtype

Due to the updating of hospital equipment, different scan protocols were applied. Imaging data were obtained using 2 different CT devices, namely, LightSpeed Ultra/Discovery HD 750 (GE Medical Systems) and Siemens third-generation dual-source CT (Somatom Force, Siemens Healthcare). All examinations (baseline and follow-up CTs) were performed in unenhanced mode with a slice thickness of 1.25 or 1.00 mm.

These thin-section CT images were reconstructed by applying a high-frequency reconstruction kernel and a lung window setting (level, −700 HU; width, 1500 HU). The SSNs were classified into 2 subtypes based on their composition: nodules without solid parts were classified as NSNs, and nodules consisting of both ground-glass and solid soft-tissue components based on attenuation were classified as PSNs.[14]

Pathological classification

The pathology slides of all nodules were reviewed initially by a primary pathologist and subsequently by a senior pathologist, according to the 2015 World Health Organization classification of lung adenocarcinomas.[15] If there was any disagreement, another senior pathologist was consulted to make the final decision. According to the pathological diagnosis, the SSNs were divided into the adenocarcinoma in situ (AIS) group (including atypical adenomatous hyperplasia, AAH), minimally invasive adenocarcinoma (MIA) group, and invasive adenocarcinoma (IAC) group.

Semiautomatic segmentation, subsolid nodules characteristics, and tumor growth patterns

The volume of each nodule was measured by 2 experienced thoracic radiologists (8 and 10 years of experience in chest radiology) on unenhanced thin-slice images using semiautomatic computer-aided volumetry software in the Syngo Via VB10 workstation (Siemens Healthcare). First, with a single click in the region of interest of each nodule, the radiologists could roughly specify the target nodule on axial, sagittal, and coronal images. Then, the program automatically segmented the target nodule based on the target nodule's attenuation value and the lung parenchymal background. If the difference between the attenuation values of the nodule and lung parenchyma was relatively small, manual adjustment of the extracted area was performed. These manual adjustments included ensuring that all areas of visible nodular opacity were included in the extracted area on axial, sagittal, and coronal images and that any adjacent structures (blood vessels and chest wall) were excluded. Representative cases of nodule segmentation are shown in Figure 2.

The relative difference (RD) overall volume between the baseline and final preoperative CTs was calculated using the formula, RD = (V1−V0)/V0, where V0 is the volume on baseline CT and V1 is the volume on final CT. If the RD was ≥25%, the solid component in the PSN had increased by 2 mm or more or a new solid component appeared within the NSNs compared with that at baseline, the nodules were categorized into the growth group, and surgery was recommended. If the RD was <25% mm^3, the nodules were categorized into the non-growth group, and follow-up monitoring was recommended.[16,17]

Each nodule was categorized in terms of its morphological features and location on multiplanar reconstruction images by the same 2 thoracic radiologists on a Syngo Via VB10 workstation. Because the imaging features of malignant nodules are highly variable, especially for SSNs, indeterminate SSNs were defined as follows: (1) nodules without definite benign features, including blurred boundaries or other inflammatory lesions in the lung; (2) nodules with a solid component ≤5 mm;[2,18] and (3) modules with no or only 1 typical morphological sign of malignancy, including a spiculated sign, lobulated sign, vacuole sign, and pleural adhesion/retraction. A consensus meeting was held to resolve any discrepancies.

Mass was calculated as M = V* (A + 1000)/1000, where M is the mass in milligrams, V is the volume in cubic millimeters, and A is the mean attenuation in Hounsfield units.[19] Volume doubling time (VDT) and mass doubling time (MDT) were calculated for any SNNs exhibiting growth as t*log2/log ($X1/X0$), where t is the interval between the final and baseline CT scans and $X1$ and $X0$ are the final and baseline volumes (or mass) at the corresponding time points.[20,21]

Statistical analysis

Data were tested for normality. Normally distributed data are expressed as the mean ± standard deviation, and non-normally distributed data are expressed as the median (range). The Bland–Altman method was applied to quantify interobserver variability. Categorical data are presented as numbers (percentages). In univariate analyses, the Mann–Whitney U test was used for nonparametric data, the independent-sample t test was used for continuous variables, and the Pearson chi-square test or Fisher exact test was used for categorical variables. Kaplan–Meier analysis and the log-rank test were performed in univariate analyses. Furthermore, multivariate Cox proportional hazards regression analysis with forward based on conditional parameter estimation selection was performed to identify independent predictors of SSN growth. All analyses were performed using Statistical Package for the Social Sciences software v. 25.0 (IBM Corp.). A two-sided P value < .05 was considered statistically significant.

Results

The present study included 24 men and 53 women (mean age of 56 years) with 80 resected SSNs (pathological diagnoses: 29 cases of AIS/1 case of AAH, 29 cases of MIA, and 18 cases of IAC). There were 13 patients with a history of smoking and 64 patients with no history of smoking. Among the 77

patients, 53 (68.8%) had more than 1 SSN. The mean follow-up period was 461.7 ± 202.5 days, and approximately 36.4% of the patients had a follow-up period shorter than 1 year; 7 SSNs from these patients showed growth. Forty-seven patients underwent lymph node dissection, and none had lymphatic metastasis.

Manual delineation of the extracted 3D area of each target nodule by the 2 thoracic radiologists took an average of 62 seconds. The mean nodule diameter on baseline CT was 9.2 ± 3.0 mm, and the median nodule volume was 234.3 mm^3 (range, 22.5-1929 mm^3). The Bland–Altman scatter plot was used to calculate the 95% CI of deviation, and the relative volume difference between the 2 readers was −5.5% to 12.3%.

In total, 63 NSNs and 17 PSNs were detected on baseline CT, and only 1 developed a new solid component. Three SSNs showed newly developed morphologic features on follow-up CT, namely, spiculation, vacuole signs, or pleural adhesion/retraction. The detailed characteristics of the 80 SSNs are listed in Table 1. Finally, 35 SSNs were classified into the growth group (growth in volume with/without the development of solid components), and the remaining 45 SSNs were observed to be stable or to show a decrease in volume and were classified into the non-growth group. Figure 3 shows a PSN from the growth group, and Figure 4 shows an NSN from the non-growth group.

There were statistically significant differences in patient's age (P = .018), morphologic features (P = .013), CT subtype (P < .001), diameter (P = .027), mean CT value (P = .009), volume (P = .032), and mass (P = .015) at baseline between the growth and non-growth groups. Patient's age (odds ratio [OR] = 1.041, P = .045) and CT subtype (OR = 3.430, P = .002) were predictors for SSN growth. In the growth group, the overall mean VDT and MDT were 811.5 days and 616.5 days, respectively. The results of the univariate and multivariate analyses to identify risk factors for SSN growth are summarized in Table 2.

The time until SSN growth is shown in Figures 5 and 6. The 360- and 720-day cumulative percentages of SSN growth were 8.75% and 35%, respectively (Figure 5). The cumulative percentages of growing SSNs were significantly different among the 3 pathological groups (P = .003), with the

Table 1. Thin-section CT characteristics of the 80 SSNs

SSN characteristics	Baseline CT	Final CT
Subtypes		
NSNs	63 (78.8)	62 (77.5)
PSN	17 (21.3)	18 (22.5)
Morphologic features		
Smooth	35 (43.8)	33 (41.3)
Spiculated sign	4 (5)	5 (6.3)
Lobulated sign	24 (30)	24 (24.1)
Vacuole sign	5 (6.3)	6 (7.5)
Pleural adhesion/retraction	12 (15)	13 (16.2)
Diameter (mm)	9.2 ± 3.0	10.1 ± 3.6
Final maximum size of the solid component within PSNs (mm)	3.5 ± 1.6	7.2 ± 3.4
Volume (mm^3)	234.3 (22.5, 1929)	289.8 (21.5, 3066)
Mean CT value (HU)	−613.4 ± 104.6	−604.6 ± 103.8
Mass (mg)	84.0 (6.6, 730.7)	127.3 (6.77, 1645.8)

Values are expressed as number (%), mean ± standard deviation, or median range.
SSN, subsolid nodule; NSN, non-solid nodule; PSN, part-solid nodule, CT, computed tomography.

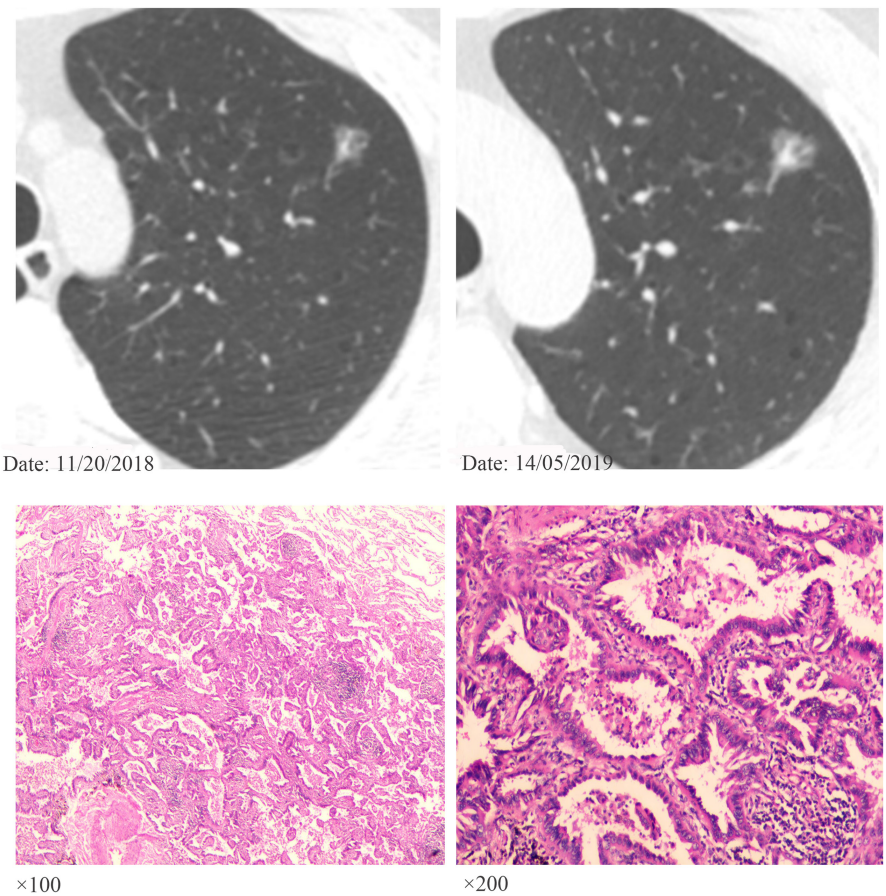

Figure 3. Representative axial CT imaging and pathologic findings (eosin staining; ×100, ×200): a part-solid nodule confirmed as minimally invasive adenocarcinoma in the growth group. Growth of the solid component and an increase in overall volume was observed during the preoperative follow-up period of 195 days. The volume and mass were 357.5 mm^3 and 136.5 mg on baseline CT vs. 1142.0 mm^3 and 487.63 mg on the final preoperative CT.

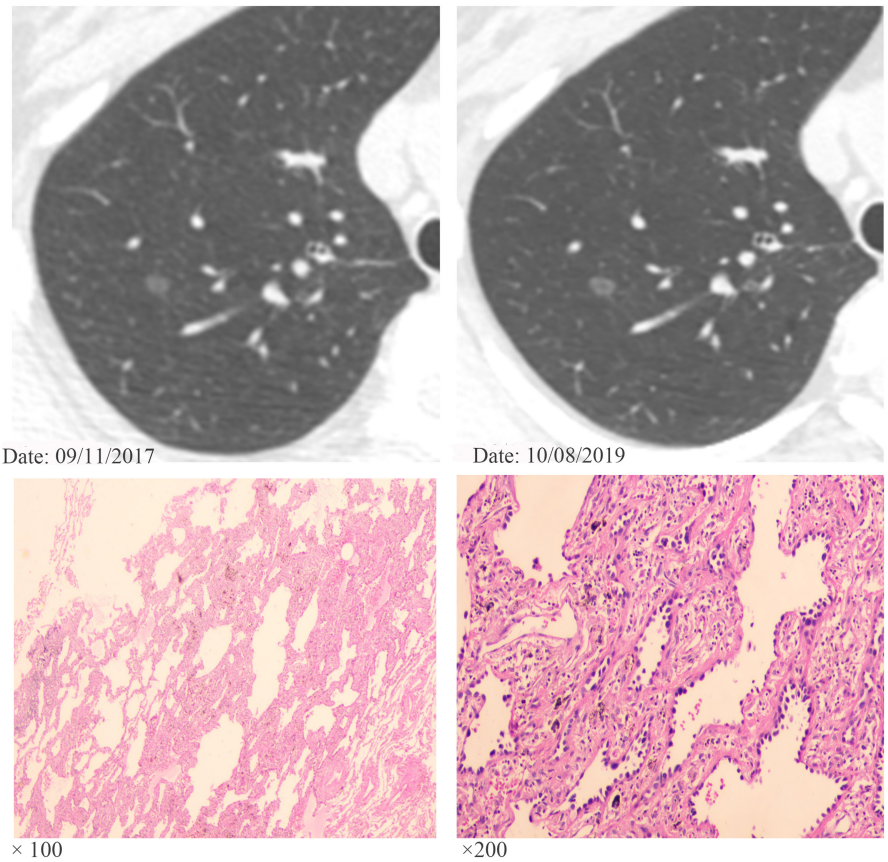

Figure 4. Representative axial CT imaging and pathologic findings (eosin staining; ×100, ×200): a non-solid nodule confirmed as minimally invasive adenocarcinoma in the nongrowth group. The volume and mass were 131.5 mm^3 and 38.00 mg on baseline CT vs. 134.0 mm^3 and 39.8 mg on final preoperative CT.

IAC group showing the highest cumulative growth percentage (Figure 6).

Compared to their appearance on baseline CT, 72.2% (13/18) of IACs, 48.3% (14/29) of MIAs, and 25% (8/32) of AISs (but not the AAH) showed growth on final CT. The baseline volume, mass, and mean CT value in the IAC group were 341.0 mm^3, 179.8 mg, and −509.7 ± 108.8 HU, which were significantly higher than those in the AIS group (101.8 mm^3, 41.9 mg, and −669.0 ± 62.2 HU, all $P < .015$), but no significant differences were found between the IAC and MIA groups or between the MIA and AIS groups. The VDT and MDT were 607.1 ± 346.7 days and 502.0 days in the IAC group, respectively, which were significantly shorter than those in the AIS and MIA groups (1300.8 ± 684.6 days, 1153.5 days and 730.6 ± 413.9 days, 516.1 days, respectively), with significant differences observed between the AIS and MIA groups ($P < .015$). Further detailed characteristics of the growth group are shown in Table 3. In addition, in the MIA group, one of the 2 PSNs developed a solid component. In the IAC group, 6 of the 16 PSNs developed a solid component, and only 1 showed NSN in baseline CT but a new solid component during follow-up CT. None of the nodules in the AIS group presented as PSNs or developed new solid components on follow-up CT.

Growth curves were plotted for the 19 SSNs showing growth with 3 or more available CT scans for comparison among the 3 pathological groups (Figure 7). Eleven nodules showed ascending curves, all of which were in either the IAC or MIA group, but the upward slope varied at each stage, with 6 showing a steep upward slope, 4 showing a gradual increase, and 1 showing a downward trend. Eight nodules showed a plateaued curve, all of which were in the AIS group, but the curve fluctuated slightly relative to the X-axis.

Discussion

The growth patterns of SSNs are still unclear, and whether the growth patterns are influenced by a previous history of malignancy remains unknown.[22] Some studies have aimed to investigate the growth patterns of SSNs; among the studies including both cancer survivors and patients without a history of cancer, the authors concluded that a previous history of malignancy could be a predictor of nodular tumor growth.[10,23-25] Some studies did not mention whether the enrolled patients had a previous history of malignancy.[26,27] One study explicitly excluded patients who had a history of lung cancer but did not clearly state whether their patients had a history of malignancies in other organs.[28] In the present study, the proportion of PSNs that grew (87.5%) was similar to that reported in some previous studies. However, the proportion of NSNs that grew (37.5%) was higher than that in Tang et al.'s[27] study (10%) but lower than that in Qi et al.'s[10] study (62.1%). We are concerned that a history of any cancer might potentially impact SSN growth patterns, especially NSN growth. Therefore, only patients without any previous malignancy were included in the present study. We believe that this additional criterion could help to better clarify SSN growth patterns, which could potentially assist radiologists, oncologists, and surgeons in managing incidental SSNs in clinical practice.

An accurate nodular volume measurement is a prerequisite for accurate assessments of nodular growth patterns. The latest nodule management guidelines from both the Fleischner Society[2] and the British Thoracic Society[29] recommend the use of volume-based measurements as the first tool for the measurement and management of pulmonary nodules. Previous studies have mostly used semiautomatic volume measurement packages to measure the volume of SSNs, and authors have reported that the combination of the semiautomatic method with radiologist input can lead to improvements in the initial automatic segmentation to separate the SSN, with good repeatability.[30,31] However, semiautomatic measurements require time and effort. In the present study, the average processing time for a nodule was 62 seconds, with the longest duration reaching nearly 3 minutes. Although this method is time consuming, good interobserver agreement for SSN volume measurements was observed in our study. Thus, we conclude that the semiautomatic method could be reliable for SSN segmentation.

Using reliable semiautomatic volume measurements, all pulmonary SSNs in the

Table 2. Univariate and multivariate analyses to identify risk factors for SSN growth

	Univariate analysis			Univariate analysis[f]	Multivariate analysis[*]	
	Growth group (n=35)	Non-growth group (n=42)	*P*	*P*	HR (95% CI)	*P*
Patient characteristics						
Sex			.653[a]			
Female	25 (71.4)	28 (66.7)				
Male	10 (28.6)	14 (33.3)				
Age (years)	58.5 ± 9.8	54.2 ± 9.4	.055[b]	.018	1.041 (1.001, 1.084)	.045
History of smoking			.956[a]			
No	29 (82.9)	35 (83.3)				
Yes	6 (17.1)	7 (16.7)				
CT characteristics						
No. of SSNs			.151[a]			
Solitary	8 (22.9)	16 (38.1)				
Multiple	27 (77.1)	26 (61.9)				
Morphologic features			<.001[c]	.013		
Smooth	7 (20)	25 (59.5)				
Spiculated sign	3 (8.6)	1 (2.4)				
Lobulated sign	17 (48.6)	7 (16.7)				
Vacuole sign	1 (2.9)	4 (9.5)				
Pleural adhesion/retraction	7 (20)	5 (11.9)				
Subtype			.036[a]	<.001		.002
NSN	24 (68.6)	37 (88.1)			Reference	
PSN	11 (31.4)	5 (11.9)			3.430 (1.603, 7.342)	
Location			.869[c]			
RUL	15 (42.9)	17 (40.5)				
RML	3 (8.6)	3 (7.1)				
RLL	6 (17.1)	7 (16.7)				
LUL	5 (14.3)	10 (23.8)				
LLL	6 (17.1)	5 (11.9)				
Baseline mean diameter (mm)	9.4 ± 2.9	9.4 ± 3.1	.074[f]	.027		
Final maximum size of the solid component among SSNs (mm)	0.0 (0.0-18.6)	0.0 (0.0-7.8)	<.001[d]			
Baseline mean CT value (HU)	−587.5 ± 107.4	−632.0 ± 102.0	.002[f]	.009		
Baseline volume (mm^3)	237.5 (43, 1929)	238.3 (22.5, 1495)	.092[f]	.032		
Baseline mass (mg)	85.5 (12, 679)	84 (6.6, 558)	.065[f]	.015		
Interval time	509.7 ± 195.6	426.6 ± 207.1	.076[b]			
VDT (days)	811.5 ± 528.2	--	NA			
MDT (days)	616.5 (106.2, 15471.4)	--	NA			
Pathologic group			.008[c]			
AAH/AIS	0 (0)/8 (22.9)	1 (2.4)/21 (50)	NA			
MIA	14 (40)	15 (35.7)	NA			
IAC	13 (37.1)	5 (11.9)	NA			

Values are expressed as number (%), mean ± standard deviation, or median (range).
HR, hazard ratio, CT, computed tomography, SSN, subsolid nodule; NSN, non-solid nodule; PSN, part-solid nodule; RUL, right upper lobe; RML, right middle lobe; RLL, right lower lobe; LUL, left upper lobe; LLL, left lower lobe; VDT, volume doubling time; MDT, mass doubling time; AAH, atypical adenomatous hyperplasia; AIS, adenocarcinoma in situ; MIA, minimally invasive adenocarcinoma; IAC, invasive adenocarcinoma. One SSN per patient (choosing the more malignant one when the patient had 2 SSNs) was used for the analysis.
[a]Pearson chi-square, [b]independent-sample t test, [c]Fisher exact test, [d]Mann–Whitney U test, [f]Kaplan–Meier analyses with the log-rank test.
*Univariate Cox proportional hazards regression analysis with forward based on conditional parameter estimation selection.

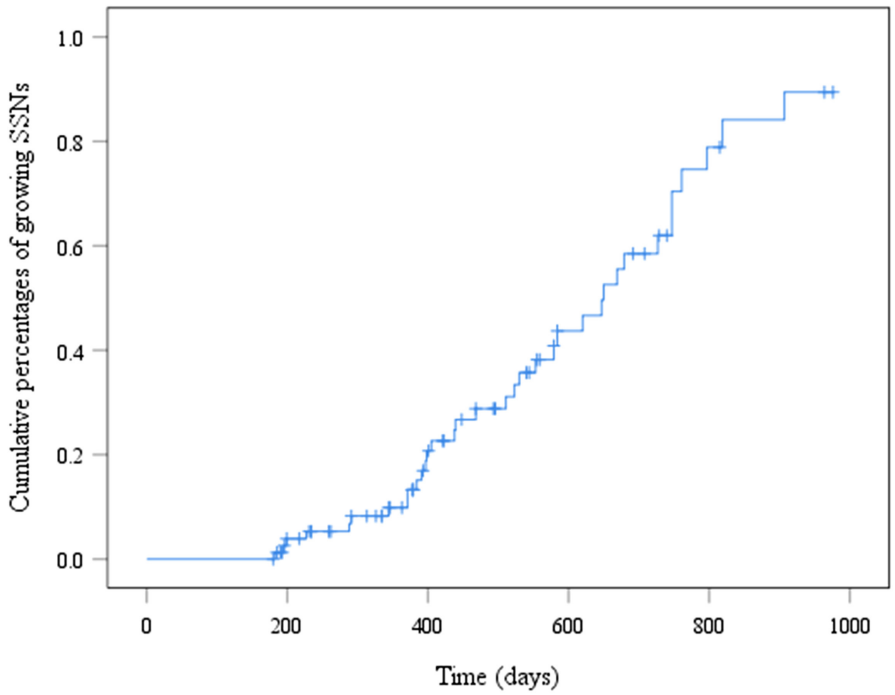

Figure 5. Kaplan–Meier curves of the time until SSN growth. For all enrolled SSNs, the 360- and 720-day cumulative percentages of SSN growth were 8.75% and 35%, respectively. SSNs, subsolid nodules.

present study were classified into a growth group (growth in volume with or without the development of solid components) and a non-growth group (stable or decrease in volume). We found that the risk of SSN growth increased with age, and PSNs were more likely to show growth than NSNs, which is consistent with some previous studies.[10,13,32]

In this study, the growth group was divided into 3 pathological groups (AIS, MIA, and IAC) according to the 2015 World Health Organization classification of lung adenocarcinomas. A previous study[10] classified SSNs into only 2 pathological groups: the non-IAC group (AIS and MIA) and the IAC group. We found that in the growth group, it was difficult to distinguish between MIA and AIS with regard to volume, mass, and CT value on baseline CT; however, there were significant differences between the AIS and MIA groups in VDT and MDT. We hope that our pathological grouping could improve imaging and treatment approaches for indeterminate SSNs in routine workflows.

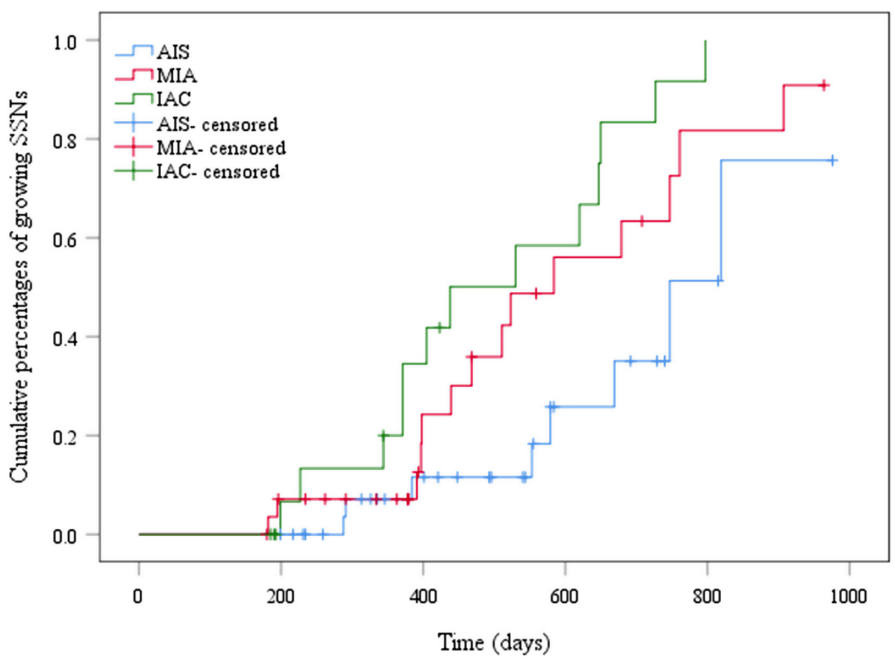

Figure 6. Kaplan–Meier curves of the time until SSN growth. The cumulative percentages of SSN growth were significantly different among the three pathological groups, and IACs showed the highest cumulative growth percentage. SSNs, subsolid nodules; AIS, adenocarcinoma in situ; MIA, minimally invasive adenocarcinoma; IAC, invasive adenocarcinoma.

Of the 19 SSNs with plotted growth curves, 11 nodules were characterized by an ascending curve (Figure 7), but the upward slope varied at each stage, demonstrating that the rate of SSN growth is not fixed but varies at different stages, consistent with some previous studies.[33-35] Although we believe that the growth patterns of SSNs may vary and that these changes might occur at different time points, further studies are needed because the number of patients with 3 or more preoperative CT scans in the growth group was small.

All enrolled patients underwent video-assisted thoracoscopic wedge or lobectomy at our hospital, of whom 16 patients underwent lobectomy. The median distance and quartile of the enrolled nodules from the pleura was 8 mm (4 mm and 7 mm). Of these, 59 patients underwent CT-guidewire localization before surgery to help surgeons accurately locate the lesions because of the distance from the nodules to the pleura or a low CT value. Five patients developed pneumothorax and required treatment after surgery because multiple bronchopulmonary segments were resected at the same time, resulting in large surgical wounds. A 70-year-old patient with coronary heart disease died of cardiac arrest on the first day after surgery. Deep venous thrombosis of the lower extremities occurred in 9 patients.

There were some limitations to this study. First, the data came from a single center, and the sample size was relatively small. Second, the resected SSN might reflect a small snapshot of the growth pattern of each SSN. Third, we used a retrospective design, not a prospective design. Fourth, we did not assess intra-observer variability in SSN volume measurements.

In conclusion, as age increases, the risk of pulmonary SSN growth increases by 4 % each year, and PSNs have a 3 times

Table 3. Thin-section CT characteristics of different pathological groups within the growth group

Characteristics	Pathological group			*P*
	AIS (n = 8)	MIA (n = 14)	IAC (n = 13)	
Baseline volume (mm^3)	101.8 (84.0, 148) *	296.5 (43, 1052)	341.0 (104.5, 1929.0) *	.005[a]
Baseline mass (mg)	41.9 (24.6, 59.4) *	117.9 (12, 389.8)	179.8 (39.6, 679.0)*	.009[a]
Baseline mean CT value (HU)	−669.0 ± 62.2 *	−614.6 ± 93.3	−509.7 ± 108.8 *	<.001[b]
VDT (days)	1300.8 ± 684.6 *	730.6 ± 413.9 * #	607.1 ± 346.7 #	.006 [b]
MDT (days)	1153.5 (405.2, 1547.4) *	516.1 (106.2, 911.7) *	502.0 (334.8, 1933.5)	.020[a]

Values are expressed as number (%), mean ± standard deviation, or median (range).
AIS, adenocarcinoma in situ; MIA, minimally invasive adenocarcinoma; IAC, invasive adenocarcinoma; CT, computed tomography, VDT, volume doubling time; MDT, mass doubling time.
*, #significant differences between groups.
[a]Kruskal–Wallis test, [b]1-way ANOVA.

higher risk for growth compared to NSNs in patients with no history of cancer. Subsolid nodules with more aggressive pathological characteristics grow at a faster rate.

Acknowledgments

We express our gratitude to Shanshan Shen, Hong Ji, Qiu Shao, Qi Zhang, Shuqian Zhang, Yingmin Chen, Fengying Zhu for data acquisition. We are grateful to Dr. Ying Wang, MD, PhD (Department of Radiology, Tianjin Medical University General Hospital) and Dr. Feng Li, MD, PhD (Department of Radiology, the University of Chicago) for her expert advice and the editing of this manuscript.

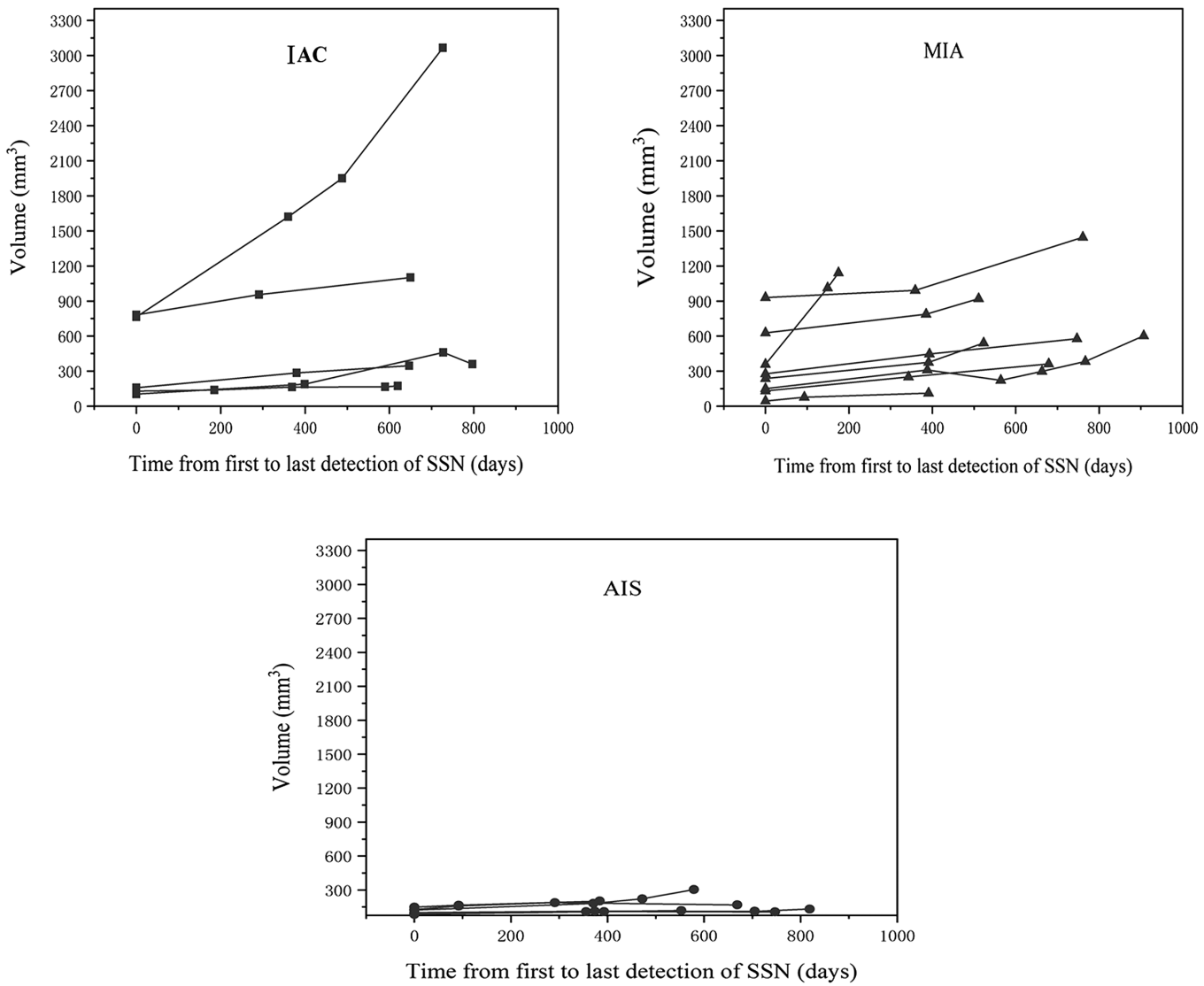

Figure 7. Growth curves by pathologic group. IAC, invasive adenocarcinoma; MIA, minimally invasive adenocarcinoma; AIS, adenocarcinoma in situ.

Conflict of interest disclosure

The authors declared no conflicts of interest.

References

1. Bueno J, Landeras L, Chung JH. Updated Fleischner Society guidelines for managing incidental pulmonary nodules: common questions and challenging scenarios. *RadioGraphics*. 2018;38(5):1337-1350. [CrossRef]
2. MacMahon H, Naidich DP, Goo JM, et al. Guidelines for management of incidental pulmonary nodules detected on CT images: from the Fleischner Society 2017. *Radiology*. 2017;284(1):228-243. [CrossRef]
3. Kim HY, Shim YM, Lee KS, Han J, Yi CA, Kim YK. Persistent pulmonary nodular ground-glass opacity at thin-section CT: histopathologic comparisons. *Radiology*. 2007;245(1):267-275. [CrossRef]
4. Kim TJ, Goo JM, Lee KW, Park CM, Lee HJ. Clinical, pathological and thin-section CT features of persistent multiple ground-glass opacity nodules: comparison with solitary ground-glass opacity nodule. *Lung Cancer*. 2009;64(2):171-178. [CrossRef]
5. Borghesi A, Farina D, Michelini S, et al. Pulmonary adenocarcinomas presenting as ground-glass opacities on multidetector CT: three-dimensional computer-assisted analysis of growth pattern and doubling time. *Diagn Interv Radiol*. 2016;22(6):525-533. [CrossRef]
6. Mackintosh JA, Marshall HM, Yang IA, Bowman RV, Fong KM. A retrospective study of volume doubling time in surgically resected non-small cell lung cancer. *Respirology*. 2014;19(5):755-762. [CrossRef]
7. Hiramatsu M, Inagaki T, Inagaki T, et al. Pulmonary ground-glass opacity (GGO) lesions-large size and a history of lung cancer are risk factors for growth. *J Thorac Oncol*. 2008;3(11):1245-1250. [CrossRef]
8. Lee HJ, Goo JM, Lee CH, Yoo CG, Kim YT, Im JG. Nodular ground-glass opacities on thin-section CT: size change during follow-up and pathological results. *Korean J Radiol*. 2007;8(1):22-31. [CrossRef]
9. Kim H, Park CM, Koh JM, Lee SM, Goo JM. Pulmonary subsolid nodules: what radiologists need to know about the imaging features and management strategy. *Diagn Interv Radiol*. 2014;20(1):47-57. [CrossRef]
10. Qi LL, Wang JW, Yang L, et al. Natural history of pathologically confirmed pulmonary subsolid nodules with deep learning-assisted nodule segmentation. *Eur Radiol*. 2021;31(6):3884-3897. [CrossRef]
11. Qi LL, Wu BT, Tang W, et al. Long-term follow-up of persistent pulmonary pure ground-glass nodules with deep learning-assisted nodule segmentation. *Eur Radiol*. 2020;30(2):744-755. [CrossRef]
12. Chang B, Hwang JH, Choi YH, et al. Natural history of pure ground-glass opacity lung nodules detected by low-dose CT scan. *Chest*. 2013;143(1):172-178. [CrossRef]
13. Silva M, Bankier AA, Centra F, et al. Longitudinal evolution of incidentally detected solitary pure ground-glass nodules on CT: relation to clinical metrics. *Diagn Interv Radiol*. 2015;21(5):385-390. [CrossRef]
14. Hansell DM, Bankier AA, MacMahon H, McLoud TC, Müller NL, Remy J. Fleischner Society: glossary of terms for thoracic imaging. *Radiology*. 2008;246(3):697-722. [CrossRef]
15. Mengoli MC, Longo FR, Fraggetta F, et al. The 2015 World Health Organization classification of lung tumors. *Pathol Int*. 2015;68:431-435. [CrossRef]
16. Xu DM, Gietema H, de Koning H, et al. Nodule management protocol of the Nelson randomised lung cancer screening trial. *Lung Cancer*. 2006;54(2):177-184. [CrossRef]
17. Field JK, Duffy SW, Baldwin DR, et al. UK Lung Cancer RCT Pilot Screening Trial: baseline findings from the screening arm provide evidence for the potential implementation of lung cancer screening. *Thorax*. 2016;71(2):161-170. [CrossRef]
18. Naidich DP, Bankier AA, MacMahon H, et al. Recommendations for the management of subsolid pulmonary nodules detected at CT: a statement from the Fleischner Society. *Radiology*. 2013;266(1):304-317. [CrossRef]
19. de Hoop B, Gietema H, van de Vorst S, Murphy K, van Klaveren RJ, Prokop M. Pulmonary ground-glass nodules: increase in mass as an early indicator of growth. *Radiology*. 2010;255(1):199-206. [CrossRef]
20. Suzuki K, Koike T, Asakawa T, et al. A prospective radiological study of thin-section computed tomography to predict pathological noninvasiveness in peripheral clinical IA lung cancer (Japan Clinical Oncology Group 0201). *J Thorac Oncol*. 2011;6(4):751-756. [CrossRef]
21. Reeves AP, Chan AB, Yankelevitz DF, Henschke CI, Kressler B, Kostis WJ. On measuring the change in size of pulmonary nodules. *IEEE Trans Med Imaging*. 2006;25(4):435-450. [CrossRef]
22. O'Dwyer E, Halpenny DF, Ginsberg MS. Lung cancer screening in patients with previous malignancy: is this cohort at increased risk for malignancy? *Eur Radiol*. 2021;31(1):458-467. [CrossRef]
23. Ichinose J, Kawaguchi Y, Nakao M, et al. Utility of maximum CT value in predicting the invasiveness of pure ground-glass nodules. *Clin Lung Cancer*. 2020;21(3):281-287. [CrossRef]
24. Cho J, Kim ES, Kim SJ, et al. Long-term follow-up of small pulmonary ground-glass nodules stable for 3 years: implications of the proper follow-up period and risk factors for subsequent growth. *J Thorac Oncol*. 2016;11(9):1453-1459. [CrossRef]
25. Kakinuma R, Noguchi M, Ashizawa K, et al. Natural history of pulmonary subsolid nodules: a prospective multicenter study. *J Thorac Oncol*. 2016;11(7):1012-1028. [CrossRef]
26. Li Q, Fan L, Cao ET, Li QC, Gu YF, Liu SY. Quantitative CT analysis of pulmonary pure ground-glass nodule predicts histological invasiveness. *Eur J Radiol*. 2017;89:67-71. [CrossRef]
27. Tang EK, Chen CS, Wu CC, et al. Natural history of persistent pulmonary subsolid nodules: long-term observation of different interval growth. *Heart Lung Circ*. 2019;28(11):1747-1754. [CrossRef]
28. Henschke CI, Yip R, Smith JP, et al. CT screening for lung cancer: part-solid nodules in baseline and annual repeat rounds. *Am J Roentgenol*. 2016;207(6):1176-1184. [CrossRef]
29. Callister ME, Baldwin DR, Akram AR, et al. British Thoracic Society guidelines for the investigation and management of pulmonary nodules. *Thorax*. 2015;70(suppl 2):ii1-ii54. [CrossRef]
30. Cohen JG, Goo JM, Yoo RE, et al. Software performance in segmenting ground-glass and solid components of subsolid nodules in pulmonary adenocarcinomas. *Eur Radiol*. 2016;26(12):4465-4474. [CrossRef]
31. Devaraj A, van Ginneken B, Nair A, Baldwin D. Use of volumetry for lung nodule management: theory and practice. *Radiology*. 2017;284(3):630-644. [CrossRef]
32. Lee SW, Leem CS, Kim TJ, et al. The long-term course of ground-glass opacities detected on thin-section computed tomography. *Respir Med*. 2013;107(6):904-910. [CrossRef]
33. Lindell RM, Hartman TE, Swensen SJ, Jett JR, Midthun DE, Mandrekar JN. 5-Year lung cancer screening experience: growth curves of 18 lung cancers compared to histologic type, CT attenuation, stage, survival, and size. *Chest*. 2009;136(6):1586-1595. [CrossRef]
34. Heuvelmans MA, Vliegenthart R, de Koning HJ, et al. Quantification of growth patterns of screen-detected lung cancers: the Nelson study. *Lung Cancer*. 2017;108:48-54. [CrossRef]
35. Mets OM, Chung KM, Zanen P, et al. In vivo growth of 60 non-screening detected lung cancers: a computed tomography study. *Eur Respir J*. 2018;51(4):8. [CrossRef]